Structurally Modulated D-π-D- A(Semiconductor) Anchoring Dyes to Enhance the Tunable NLO Response: A DFT/TDDFT Quest For New Photovoltaic Materials

Abrar U. Hassan (hassanabrar2016@gmail.com)
University of Gujrat
Sajjad H. Sumrra
University of Gujrat
Muhammad Zubair
University of Gujrat
Ghulam Mustafa
University of Gujrat
Muhammad F. Nazar
University of Education
Muhammad N. Zafar
University of Gujrat

Research Article

Keywords: Semiconductor anchoring, NLO, TD-DFT, NIR, UV-Vis

Posted Date: July 15th, 2022

DOI: https://doi.org/10.21203/rs.3.rs-1813028/v1

Structurally Modulated D-π-D- $A_{(Semiconductor)}$ Anchoring Dyes to Enhance the Tunable NLO Response: A DFT/TDDFT Quest For New Photovoltaic Materials

Abrar U. Hassan,[*1] Sajjad H. Sumrra[1], Muhammad Zubair[1], Ghulam Mustafa[1], Muhammad F. Nazar[2], Muhammad N. Zafar[1]

[1]*Department of Chemistry, University of Gujrat, Gujrat 50700, Pakistan*
[2]*Department of Chemistry, Division of Science and Technology, University of Education, Lahore, Multan Campus 60700, Pakistan*

Abstract

In this paper, we show that dyes with anchoring groups and their stability for semiconductor TiO_2 surfaces with silyl unit in dye-sensitized solar cells (DSSCs). To investigate the efficacy of DSSCs, Density Functional Theory (DFT) calculations were conducted with novel D-**π-**D-$A_{(Semiconductor)}$ type dyes with using donors (*N*,*N*-dimethylaniline & benzenesulfonate) and a thiophene as π-conjugated spacers, with different semiconductor units as anchoring and electron acceptor units to design dyes (**D-1** to **D-5**). All new Dye as a reference **(Ref-D)** had been extended with electron acceptor semiconducting units to improve the electronic transmission and increased maximum absorbance (λ_{max}). Their ionization potentials ranged between 2.65-5.31ev which showed their good electron donating nature. The λ_{max} values of dyes D-1 to D-5 were 458-521 nm which had a considerable red shift from Ref-D. The second order NLO response of 134532 Debye-Angstrom^{-1} was noted for D-2 which had the shortest bandgap. The charge tripping analysis of all the dyes miscible with the Ref-D showed an exclusive shift from HOMO of reference to LUMO of dye. The density of states (DOS) calculations with the illustrative dye D-5 show that electronic transmission from the dye towards the semiconductor was efficient. The inclusion of thiophene as π-conjugated spacer resulted in a significant increase in absorbance peak at 80 nm, which have led the UV ranges to the UV-vis and NIR regions. The DFT computed results offer light upon that design of novel DSSCs with silyl anchoring groups for improved stability and efficiency. The present research is in a kind of prediction to develop new NLO materials with D-**π**-A design involving semiconductor as anchoring groups to attach with a surface.

Keywords: Semiconductor anchoring, NLO, TD-DFT, NIR, UV-Vis

Email for correspondence: hassanabrar2016@gmail.com

Introduction

The scientific pursuit for nonlinear optical (NLO) materials which are essential in present photonics [1], optical communication system [2] , and quantum chemical measurements [3], is a major topic in materials research. the fast advancement of optical science and technology has necessitated the establishment of innovative NLO materials with broader application capabilities [4]. The use of environmentally friendly renewable energy sources is of recent attention, and the issue is to improve in technology to satisfy the required demand [5]. Photovoltaic sensitive chemical dyes are one of the most promising potential renewable sources for harvesting solar energies to meet our requirements [6]. Gratzel et al. was the first to develop photosensitizer solar cells (DSSCs) as an innovative source of energy to traditional inorganic silicon-based photovoltaic modules [7]. Manufactured NLO materials in the deep ultraviolet (UV) and near-infrared regions ranges are a few [8]. The difficulty stems from the specific wavelength requirements and expensive exploration techniques. Metal-containing dyes have a greater potentials due to very broad absorbance range from UV-visible to near-infrared [9]. According to a recent study, using a co adsorbent, ruthenium-containing dye may be increased [10]. The increased PCE created by metal-based dyes is difficult to synthesize, and the supply of Ru is restricted [11]. Such dyes also get leached from the semiconductor surface to make them environmentally unfriendly [12]. As a result, solar cells dyes without any metals are a basic requirements for the viable green photovoltaics [13]. A great number of metal free dyes for solar cells application are designed by fabricating various electron poor and electron rich systems with a basic of design of Donor(D)–(π-spacer)–Acceptor(A) to attach with an electrode surface [14].

A dye chromophore, which is anchored upon that electrode surfaces, absorbs the light energy as the initial step inside the DSSC [15]. The charge separation is achieved next [16], followed by photo-induced electronic injection at the interface of the dye and semiconductors interface [17], and the content related electron is inserted into the conductive band of TiO_2 [18]. The D—π—A framework offers fair opportunities for modulating and optimizing improved efficiency in the DSSC system [19]. Specific units on a dye can be tuned to influence the electromechanical and optoelectronic properties characteristics of dye molecules [20]. The donor, π-spacer, and anchorage components have been modified to produce more efficient photovoltaic solar modulation [21]. A reduced HOMO-LUMO energy bandgap has been considered to enhance NLO

performance by enhancing electronic transition efficiency and decreasing the dye workflow [22]. The anchoring groups with their ability to bond with the electrode surface is also critical for all real-world applications [23]. Increased binding in involving anchor with the Titanium (Ti) contained on the layer of the semiconductor ensures pertinent stability of the DSSCs and improves the rate of electron flow from dye to a semiconductor wafer or anchoring unit [24]. Various anchoring groups have recently been investigated which have been attributed to the prevalence of the robust electron-withdrawing units to act as electron carrier for establishing a relation to semiconductor surfaces [25].

One of several key issues with DSSCs was the destabilization of the cyanoacrylic acid component in moisture [26]. It has been observed that in the case of moisture in an electrolytic solution, a dye containing an anchoring may easily be released from its site [27]. Organosilicon compounds are reported to have a high binding affinity to anchoring surfaces by forming of Si–O–M type linkages [28]. There are various comparison investigations that employ ethoxysilyl groups as anchors, such as 4-Triethoxysilyl)azobenzene [29], diethoxyphenylsilyl)azobenzene [30], and triethoxysilane [31] . In this study, we prove that the use of different anchoring groups as semiconductor material surfaced units in DSSCs to stabilize for semiconductor surfaces than dyes with some newly presented anchoring groups. Density functional theory (DFT) based designs were adopted using straightforward donor (N,N diphenylamine) and π-conjugated spacers with anchoring units to examine the effectiveness of DSSCs with anchoring units.

Computational methodology

The present analysis was conducted using multiple long-range and range separated DFT driven functional with Gaussian 09 application [32]. The metrics for the dyes with a very D-**π**-D-$A_{(Semiconductor)}$ designs were studied with their Frontier Molecular Orbitals (FMOs), Natural Bond Orbital (NBO), Density of State (DOS) studies, simulated UV-visible spectral analysis, and Non Linear Optical (NLO) properties in a gas and a solvent (Chloroform).

An FMO investigation was used to figure out the energy bandgap, allowing the minimal energy required for the switch from HOMO to LUMO to be decided [33]. The hyperconjugative linkages and intra-molecular charge carriers were found using an NBO method [34]. The distribution of energy states was computed using the DOS computations.

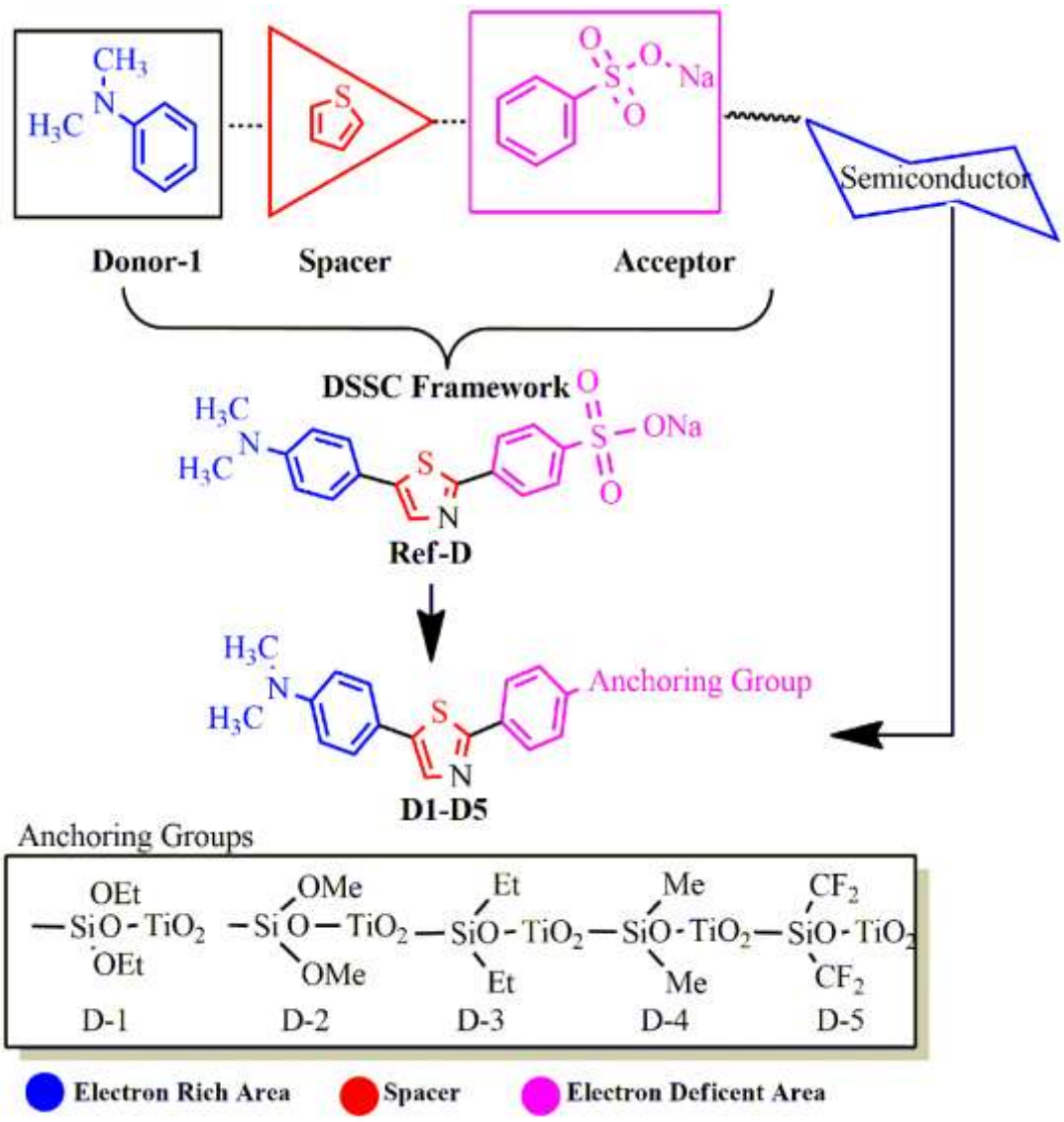

Fig. 1. Design of new D-**π**-D- $A_{(Semiconductor)}$ type dyes (D-1 to D-5) with new silyl anchoring groups

To study charge transfer, the UV visible absorption spectra were obtained. The NLO and dipole moments of the dyes were calculated from the results of the dyes in solvent. Results from extracted data using the GaussView, Avogadro, and Chemcraft programs were used to derive the conclusions. While researching the Global Reactivity Parameters (GRP), such as Electron Affinity (Ea), Global Electrophilicity Index (ω), Ionization Potential (I1), Global Chemical Potential (μ), Electronegativity (χ), Global Hardness (η), and Global Softness (σ), the E_{LUMO} and E_{HOMO} have

been used to depict reactivity and stability [35]. The following formulas are used to decide various parameters utilizing Koopman's theory [36].

$$\mathbf{I1} = -\mathrm{E_{HOMO}} \qquad \text{(Eq. 1)}$$

$$\boldsymbol{Ea} = -\mathrm{E_{LUMO}} \qquad \text{(Eq. 2)}$$

$$\boldsymbol{\chi} = \left(\frac{\mathbf{IE+EA}}{\mathbf{2}}\right) \qquad \text{(Eq. 3)}$$

$$\boldsymbol{\eta} = \frac{1}{2}\mathrm{E_{LUMO}} - \mathrm{E_{HOMO}} \qquad \text{(Eq. 4)}$$

$$\boldsymbol{\mu} = -\left(\frac{\boldsymbol{IE+EA}}{\mathbf{2}}\right) \qquad \text{(Eq.5)}$$

$$\boldsymbol{\sigma} = \frac{1}{2\eta} \qquad \text{(Eq. 6)}$$

A single-molecular system keeps track of energy constancy according to Parr's definition when it picks up extra charge on the surface out of its environment. It keeps an eye on energy consistency, according to Parr. Reactivity has a quality that makes it possible to classify things quantitatively.

$$\boldsymbol{\omega} = \left(\frac{\boldsymbol{\mu^2}}{\boldsymbol{2\eta}}\right) \qquad \text{(Eq.7)}$$

Reactivity has a quality that makes it possible to classify things quantitatively. Another essential part that affects optical performance is the effectiveness of light harvesting. The highest charge-transfer sensitivity is seen in dyes with a high LHE concentration. The formula may be used to calculate the LHE of dyes (2.9).

$$LHE = 1 - 10^{-f} \qquad \text{(Eq. 8)}$$

Open Circuit Voltage (Voc), a crucial measure for assessing the cost effectiveness of semiconductors technologies, is often calculated using the formula below.

$$V_{OC} = \frac{1}{e}([\mathrm{E_{HOMO}(D)} - \mathrm{E_{LUMO}(D)}]) - 0.03 \qquad \text{(Eq. 9)}$$

The sum of the dyes was calculated using equations (10) and (11). employing their tensors, polarizability/hyperpolarizability.

$$<\alpha>=1/3(\alpha_{xx}+\alpha_{yy}+\alpha_{zz}) \qquad \text{(Eq. 10)}$$

$$\beta_{tot} = \left[\left(\beta_{xxx}+\beta_{xyy}+\beta_{xzz}\right)^2+\left(\beta_{yyy}+\beta_{xxy}+\beta_{yzz}\right)^2+\left(\beta_{zzz}+\beta_{xxz}+\beta_{yyz}\right)^2\right]^{1/2} \quad \text{(Eq. 11)}$$

Finding chemical bonds in designed dye materials that come from hyper conjugated interactions is made easier by NBO studies. As the transition from being electron donors to becoming electron acceptors, it offers a realistic view for analyzing intra-molecular delocalization and electron density. The interaction between the electron donor functions is increasingly important as stabilization energy increases. The stabilizing energy equation using a 2nd perturbation technique is Equation 12.

$$E^{(2)} = q_i \frac{\left(F_{i,j}\right)^2}{\varepsilon_j - \varepsilon_i} \qquad \text{(Eq. 13)}$$

Results and discussions

The developed DSSCs with anchoring units were studied in their D-**π**-D- $A_{(Semiconductor)}$ designs. For theoretical ease, simple *N*,*N*-dimethylaniline was used as the electron donor group in the dyes examined. First, a Methyl Orange (MO) inspired reference dye (Ref-D) was designed in which the azo unit was converted into a spacer because azo units are often linked with their unstable nature. The Ref-D was then further structulayy modulated to create 6 new dyes (D-1-D-5) which had a Donor , A pi-spacer, another donor and a linked anchoring units with electron accepting ability. We proposed silicone based anchoring acceptors diethoxy(oxido(oxo)titanio)silane (**A1**), dimethoxy(oxido(oxo)titanio)silane (**A2**), dimethyl(oxido(oxo)titanio)silane (**A3)**, diethyl(oxido(oxo)titanio)silane (**A4**), and (oxido(oxo)titanio)bis(trifluoromethyl)silane (**A5**) as previously they are proved with good actions. Similarly, efforts were made to investigate the significance of the anchoring groups in the DSSCs efficiencies. We choose Ref-D as a reference system to investigate the parameters given and to carry out the proposed DSSCs for further investigation (Fig. 2).

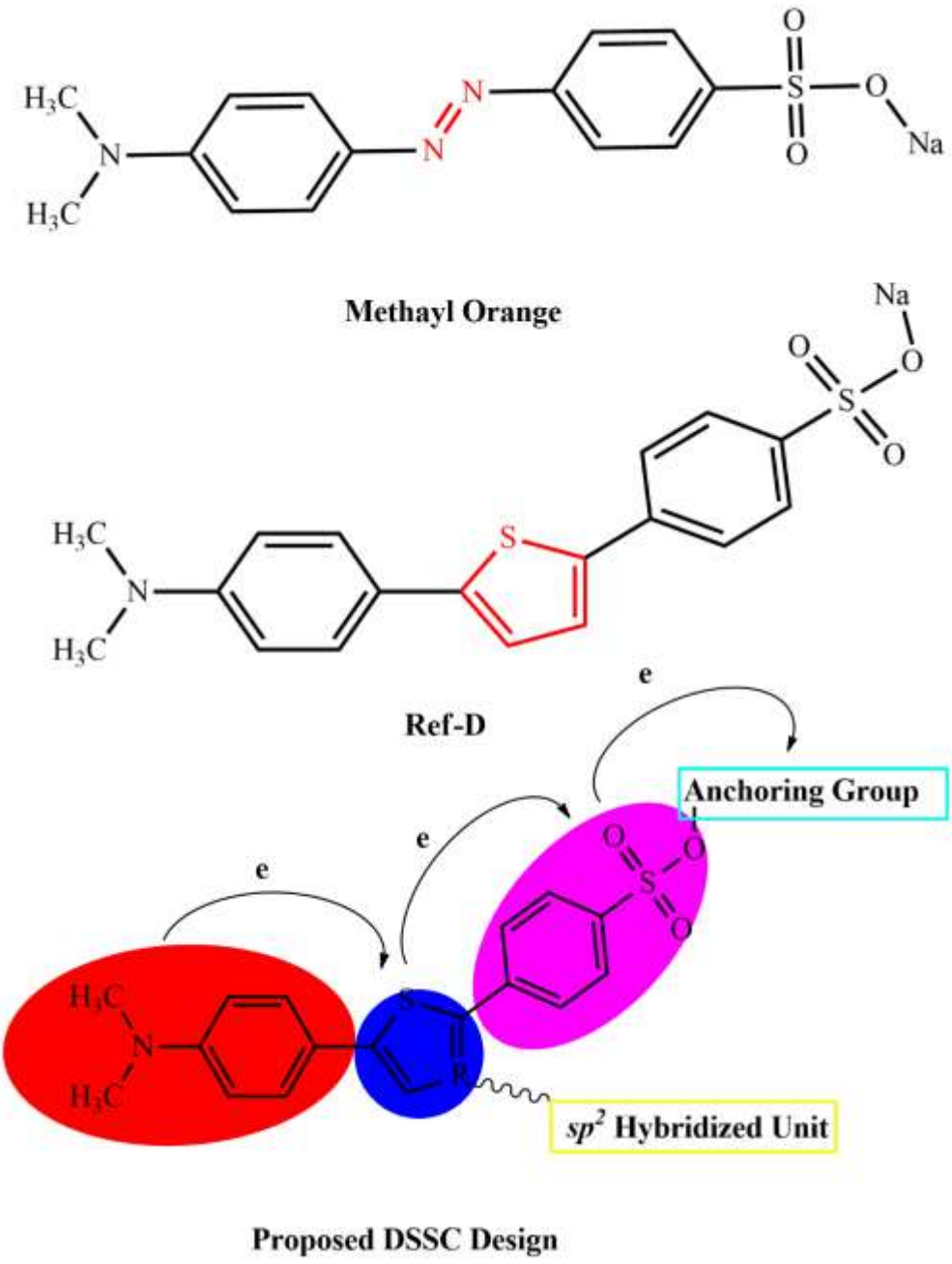

Fig. 2. Proposed designs of the reference dye (Ref-D) and its derived dyes (D-1 to D-5)

Because the azo-unit in the reference system is recognized to be reactive across a wide range of experimental circumstances, Dye-A was created with thiophene π-spacer to evaluate the efficacy of such DSSCs to the earlier dye system. The thiophene π-spacer was further accompanied by the doping of some sp^2 hybridized small units to further tune the photovoltaic performances. The introduction of a thiophene unit as a π-spacer group increases electron–hole, open-circuit voltage,

and electron injection/hole characteristics for Dye-A. Thiophene has already been stated in the literature to be a superior spacer character over benzene. We used thiophene as a spacer to investigate the factors influenced by such a group. In dye D-1, the maximum value (λ_{max}) shifts to a longer wavelength, while the other characteristics are still the same as in Dye-1. *N*,*N*-dimethylaniline serves as a donor group in all of the newly developed dyes, while thiophene is connected to thiophene as a spacer unit. To investigate the difference in the electronic dispersion of the proposed dye systems, the silyl anchoring group as acceptors were used with electron-donating (-OEt, -Me, and -Et groups) or electron-withdrawing (-CF_3 groups). In the instance of D-1, electron-donating –OEt groups are connected to the anchoring unit of Si atom. We modelled the Si anchoring group using the electron-donating methyl (–Me), ethyl (–Et), and electron-withdrawing (–CF_3) groups, which correspond to dyes 2, 3, and 4, respectively

Orientation of dyes

To get a decent NLO efficiency from donor- π linker-acceptor type dyes, the π-spacers must be evaluated. The purpose of this research is to design new possible NLO materials with various -bridges and predict their photoactivity, electronic, plus NLO properties for contemporary optical devices. For theoretical construction, a synthetic heteroaromatic PB devoid of metals was used. These dyes were composed of three main parts that worked as a pi bridge when combined. The C-C and C-H bonds are predicted to have lengths of 1.42 to 1.52 and 1.09 to 1.11, respectively. C(5)-N(13) and C(6)-N(37) had bonds that were 1.46 and 1.59 long. When considering the various angles, the calculated angles were remarkably like one another, except for around the CF3 group substitutions. The ring symmetry may be affected by the charged particle moieties on the aromatic rings, resulting in in-ring angles that are slightly more than 120° at the meta and ortho sites and slightly less than 120° at the modification point. Similar results were seen for the bond angles of C(1)-C(6)-C(5) in Ref-D, which were 118.89°, C(5)-C(13)-N(17), and C(3)-C(9)-N(4), which were 143.1° and 120.0°.The imidazole ring and pyrimidine atoms C(7)-C(8)-N(33), C(1)-C(6)-N(6), and C(11)-C(12)-N(26) have corresponding bond angles of 120.7° and 121.3°. The structural composition of the azole moiety was significantly altered by the inclusion of large donor atomic units, but the geometric conformation of the aromatic rings was left unaltered

Table 1. Structural parameters like bond lengths (A) and bond angles (°) of optimized structures of reference dye **(Ref-D)** and new dyes **(D-1 to D-5)**

Dyes	Bond Lengths (A)		Bond Angles (°)	
Ref-D	R(1-2)	1.52	A(2-1-3)	117.3
	R(6-8)	1.41	A(27-2-28)	108.2
	R(6-33)	1.13	A(29-3-30)	108.2
D-1	R(1-2)	2.07	A(2-1-3)	109.8
	R(1-3)	2.07	A(2-1-22)	108.9
	R(12-23)	1.51	A(7-8-10)	119.9
D2	R(4-7)	1.49	A(5-4-7)	119.7
	R(5-30)	1.11	A(4-5-30)	111.3
	R(5-31)	1.11	A(4-5-31)	110.2
D3	R(2-32)	1.12	A(1-2-33)	112.9
	R(2-33)	1.12	A(1-2-34)	112.0
	R(2-34)	1.12	A(23-1-30)	106.7
D4	R(1-30)	1.11	A(1-21-2)	110.8
	R(2-21)	1.88	A(1-21-20)	108.6
	R(2-31)	1.11	A(1-21-22)	110.3
D5	R(3-4)	2.07	A(29-1-32)	110.2
	R(3-5)	2.07	A(21-2-30)	111.4
	R(3-22)	2.07	A(21-2-31)	110.0

The development of dyes with varying acceptor atoms involved the use of two phenyl-conjugates. The benzene ring of Ref-D with its dihedral angle was found to be between 117.65° and 118.09°. It was found that the linked bond angles for C-C-N were 106° and 110°, respectively. The longitudinal benzene rings were found to be equivalent between 112.43° and 113.03°. The thiazole-facing benzyl circle C-C-C had a dihedral angle with 120°, so while the anchoring side side had such a geometrically exact displacement of 108°. The dihedral angles of C-C-N in the pyrrole part and C-N-N in the thiophene unit were, respectively, 106.43°-106.65° and 110.34°-110.39°.

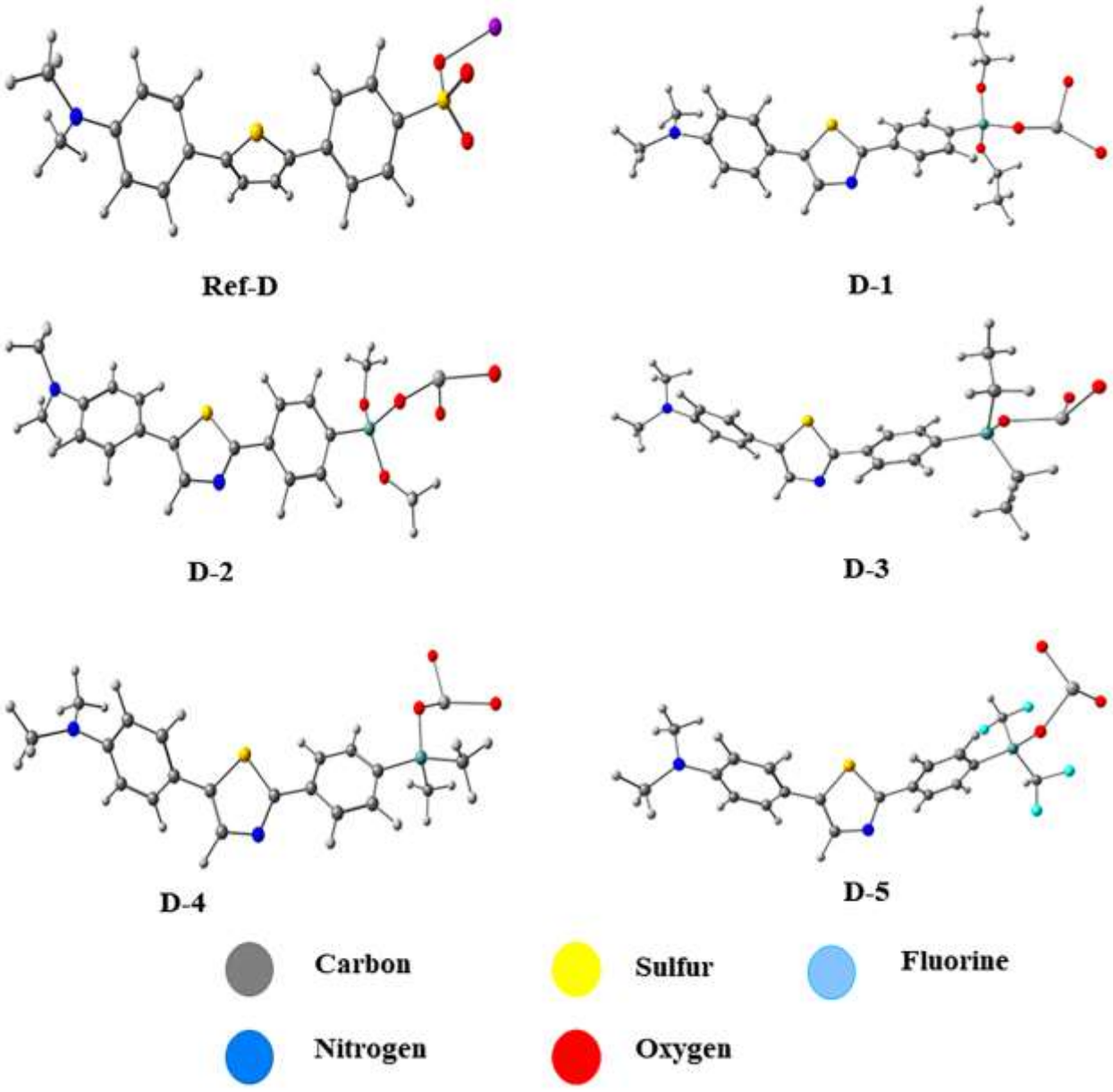

Fig. 3. Optimized geometries of reference dye **(Ref-D)** and new dyes **(D-1 to D-5)** at DFT level

Frontier Molecular Orbitals

A charge analysis of Frontier Molecular Orbital (FMOs) is crucial for predicting the chemical properties, physical permanence, electro-optic properties, and electronic wavelength of materials [37]. The acronyms for HOMO and LUMO stand for the propensity to take and distribute electrons, respectively. The dyes with their electron-poor part are represented by the LUMO, while

its electron-rich part is represented by the HOMO (Fig. 4). The proposed CT interaction of the dyes can be explained by a lower energy gap (HOMO-LUMO). There are 215 MOs in the Ref-D structure, 151 of which are occupied, and 64 of which are unoccupied. It is possible to see where the HOMO and LUMO are found across the dye materials. This suggests that HOMO and LUMO have a substantial orbital overlap, allowing the transition from GS to ES. 2.70 to 2.81 eV are the calculated HOMO/LUMO energies and their gaps.

When calculating the reactivity coefficients using Koopmans' theorem, the HOMO/LUMO interactions are taken into consideration. To investigate the kinetics of compounds in diverse zones and be able to understand some factors associated with the respondents, it is significant to use DFT-based global reactivity requirements, such as I1, μ, Ea, χ, ω, electron-donating and electron-accepting (+) power, as well as η. The LUMO and HOMO values control the Ea and I1, which are like dye materials due to their electron-accepting and -donating characteristics. The I1 value decides the ability to donate electrons, and I1 = 5.68 eV shows that dye D-4 has a very good donating capability. The D-2 may be employed in CT related applications as per its higher positive (EA) score. The HOMO orbitals were scattered around the system in dyes, although it was focused on the donor part and -bridge in Ref-D dyes from dyes D-1 to D-5. On the other side, the LUMO was discovered on the -bridge together with all the colors. The investigation showed a significant value since it affects how quickly a photosensitive dye may be duplicated throughout its electron transfer process. An electron-donating strategy that increases the HOMO energy level while also increasing the LUMO energy output can change the donor moiety (Table 2).

Table 2. Energies of Highest Occupied and Lowest Unoccupied orbitals (HOMO-LUMO) with their energy gaps (E_{H-L})

Comp.	$\mathbf{E_H}$	$\mathbf{E_L}$	$\mathbf{\Delta E_{H-L}}$
Ref-D	-5.31	-1.98	3.33
D-1	-2.66	-0.38	2.28
D-2	-2.75	-0.42	2.34
D-3	-2.67	-0.25	2.42
D-4	-2.65	-0.25	2.39
D-5	-2.70	-0.04	2.66

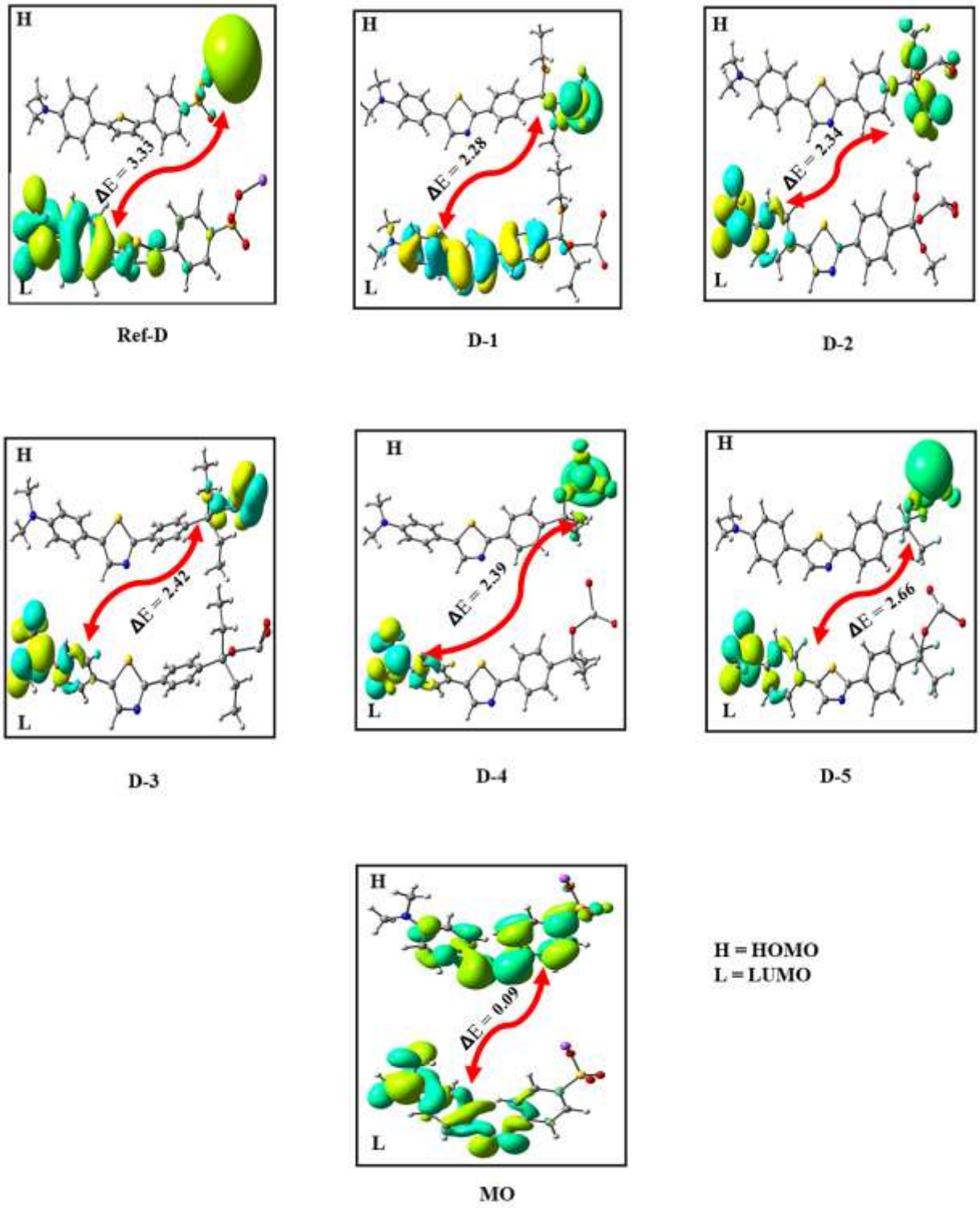

Fig. 4. An analysis of Frontier Molecular Orbitals (FMOs) of reference dye **(Ref-D)** and new dyes **(D-1 to D-5)**

The Electronic charge density diminishes because of the increasing photogenerated electron pushing power (energy differential between the LUMO and HOMO conduction and valence bands). In this investigation, the driving force of charge transfer increases as electronic charge density diminishes As the electron density distribution over the HOMO and LUMO energy orbitals is essential for deciding the electrical behavior of the intended and reference compound Ref-D, the HOMO and LUMO of dyes were also referred as the valence and conductivity bands. While LUMOs are linked to anti-bonding tendencies, HOMOs have a bonding disposition. We show how the global reactivity parameters, and the electron density transfer functions affect the distribution of frontier molecular orbitals (FMOs). Between 54 and 99 percent of electrons were transferred in exciting states with B3LYP functioning. For the dyes D-1 to D-5, the energy gaps (Eg) for the highest to lowest unoccupied orbitals (E_{HOMO}-E_{LUMO}) were 5.76 eV and 0.74-2.43 eV, respectively. All the dyes showed lower E_{H-L} values than Ref-D (3.43 eV), except for dye D-3, showing their superior electronic conduction capabilities. The difference between Ref-D indicated that there was considerable intramolecular charge transfer (ICT), which caused the absorbance values to move towards to redshift. The dye Ref-D with end-capped silyl unit had a clearly strong electron-accepting action, which caused dye D-2 and D-5 to have lesser electron-accepting actions. The dye D-3 even from the reference Ref-D was a clue that the location and number of semiconductors are very important factors to consider when building unique OSCs like patterns. Various Ns and comparable patterns to the reference were also present in other dyes. The compounds of the thiazolidine acceptor in dye D-5, as well as the dyes had strong electron acceptors and a narrower bandgap than others, showing how adding more Ns has decreased the E_g by misrepresenting the pattern of their electronic states.

Global Chemical Reactivity

Analyzing FMOs is a useful method for knowing out how stable and photovoltaic a chemical is. An essential issue in absorption spectra for the physical modelling of material is the charge distribution studies over the FMOs, from HOMO to LUMO. The most crucial factor in figuring out the stability and chemical reactivity of new compounds is the bandgap (E_{LUMO}-E_{HOMO}). Smaller E_{LUMO}-E_{HOMO} gaps are related to more reactive, less stable, and softer dye materials that are more polarized and start acting as a finer new competitor in supplying the best NLO response. In contrast, improved HOMO-LUMO prototype for a dye is related with its inertness, more

consistency, and hard dyes. To take advantage of its relevance for their promising photoluminescence, the energy gap across atomic orbitals was computed. Table 1 shows that D-4 has the lowest bandgap (0.84 eV) out of everyone due to having the π-conjugated link and anchoring gropus. Furthermore, after D-4 and D-5, which had two π-spacers and two and three acceptors, respectively, were more reactive. With phenyl π-spacers to close the energy gap, silyl anchoring groups as electron acceptors had the greatest outcomes, according to the growing bandgap ordering of such dyes. 0.84-3.67 eV (Table 3). Additionally, it was found that dyes with more π-spacers had bandgaps that were smaller, which stabilized a dye material more. Overall, the highest energy gap was discovered in D-3 (3.67 eV), while the lowest bandgap was discovered in **D-4** (0.84 eV). All analyzed dyes with I1 bandgaps are ranked according to their evaluation. Figure 2 shows the results of a study on the charge distributions on the surfaces of orbitals. In HOMOs, the charge concentrations were uniform across the dye structure; in LUMOs, however, the charge densities are at the acceptor moiety and across π-spacers.

Table. 3. Global Reactivity Parameters (GRPs) of dye Ref-D and its new dyes **(D-1 to D-5)**

Comp.	**IP**	**EA**	χ	μ	η	σ	ω
MO	0.86	0.77	0.82	-0.82	0.05	11.06	7.42
Ref-D	5.31	1.98	3.64	-3.64	1.66	0.30	3.98
D-1	2.66	0.38	1.52	-1.52	1.14	0.44	1.01
D-2	2.75	0.42	1.59	-1.59	1.17	0.43	1.08
D-3	2.67	0.25	1.46	-1.46	1.21	0.41	0.89
D-4	2.65	0.25	1.45	-1.45	1.20	0.42	0.88
D-5	2.70	0.04	1.37	-1.37	1.33	0.38	0.70

The E_{LUMO}-E_{HOMO} was used to stand for reactivity and stability by examining the Global Reactivity Parameters (GRP), which include such parameters as I1, Ea, χ, η, μ, ω, σ. The outcomes for the dyes under investigation were calculated from their molecular orbital analysis using the proper quantum chemistry implications. The ability of a substance to donate and take electrons was figured out by its I1 as well as by measuring the amplitudes of its Ea values. The energy needed to remove one electron out of a dye is represented by the I1. Increased I1 values imply stronger chemical stability and barrier properties. The I1 value for Ref-D was 5.31 eV, while the value for D-4 was 2.65 eV. Their overall ranking was determined to be as: **Ref-D** (5.31) > **D-2** (2.75) > **D-**

5 (2.7) > **D-3** (2.67) > **D-1** (2.66) > **D-4** (2.65) . Additionally, **Ref-D** had an Ea value of 1.98 eV, the highest value, while D-5 value was just 0.04 eV. Overall, it was noticed that was noted as: **Ref-D** (1.98) > **MO** (0.77) > **D-2** (0.42) > **D-1** (0.380 > **D-3** (0.25) > **D-4** (0.25) > **D-5** (0.04). The results have suggested that the Ref-D and all the dyes had exceptional electron-accepting ability since the I1 values were discovered to be much greater than the Ea values. When evaluating μ, dyes with their chemical stability is considered. The overall descending order for all the dyes was compiled as: **MO** (-0.82) > **D-5** (-1.37) > **D-4** (-1.45) > **D-3** (-1.46) > **D-1** (-1.52) > **D-2** (-1.59) >**Ref-D** (-3.64). This has also to do with the χ of dyes, whereby low values show an easy uptake of electrons and describe electron attractions. The order of the dyes overall was determined to be: **Ref-D** (3.64) > **D-2** (1.59) > **D-1** (1.52) > **D-3** (1.46) > **D-4** (1.45) > **D-5** (1.37) > **MO** (0.82)**.** The examined dyes' higher η values suggest that they are stable, as shown by the dyes with negative μ values. Their overall order was noted as: **Ref-D** (1.66) > **D-5** (1.33) > **D-3** (1.21) > **D-4** (1.2) > **D-2** (1.17) > **D-1** (1.14) > **MO** (0.05). As softness is related inversely with the hardness, its order was reversal of the hardness values order. The overall descending order was noted as: **MO** (11.06) > **D-1** (0.44) > **D-2** (0.43) > **D-4** (0.42) > **D-3** (0.41) > **D-5** (0.38) > **Ref-D** (0.3). The order of the dyes with increasing energy gaps matched the progression of their relative η. The electrophilicity was found in its decreasing order as: **MO** (7.42) > **Ref-D** (3.98) > **D-2** (1.08) > **D-1** (1.01) > **D-3** (0.89) > **D-4** (0.88) > **D-5** (0.7). This design was perfectly following the HOMO-LUMO bridging, proving that compounds with a substantial E_g value are regarded hard dye materials, having stronger stability, reduced reactivity, and resistant to electronic conformational change. The general ranking was as follows: the σ, which is related to its μ, is an added consideration. D-2 (0.27) is the least reactive part and has the lowest σ value, while **D-4** (1.19) is the most reactive dye materials and has the highest σ value, according to the rising ordering of σ values, which is in direct contrast to the expanding energy gap order:). Characteristics of global reactivity showed a strong correlation with the HOMO-LUMO bandgap order.

UV-Visible analysis

Any photovoltaic system is a semiconductor that converts light energy into electrical energy [13]. This causes electrons from the valence band moving to the conduction band [38]. The optical characteristics of photovoltaic panels are widely studied using UV/Vis/NIR spectroscopic techniques. The results showed that **Ref-D** had a red shift for the λ_{max} in comparison to **MO** (**Fig.**

5). however, the inclusion of sp^2 hybridized atom in the π-spacer part reduces the HOMO-LUMO energy gap, causing the λ_{max} to shift to a higher wavelength (red shift).

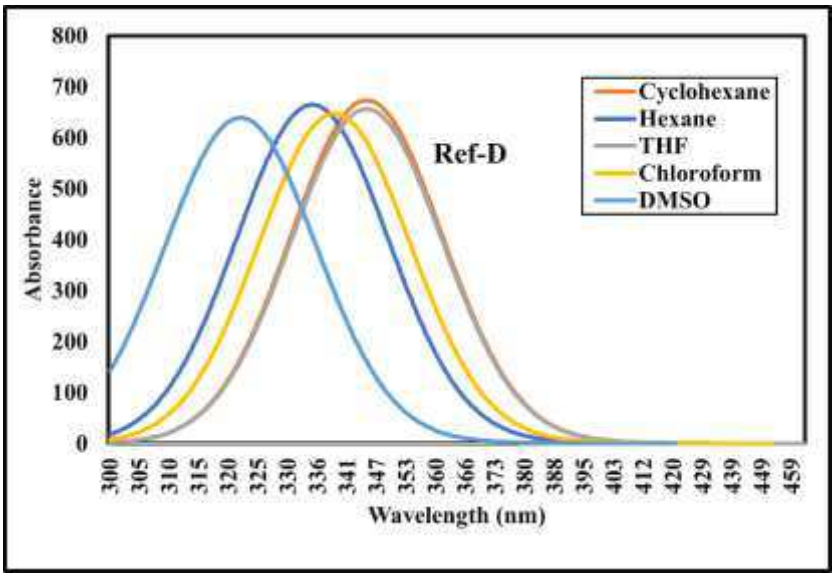

Fig. 5. Computed Uv-vis analysis of reference dye (Ref-D) under different solvents

Furthermore, the efficiency of cyanoacrylic acid and Si-containing anchoring sites was compared using an experimentally documented dye with *N*,*N*-dimethylaniline as the donor, thiophene as a π-spacer, and cyanoacrylic acid as an anchor unit. The **Ref-D** had also been estimated at the same theoretical level. In gaseous, the largest MO value is 398 nm (Fig. 6).

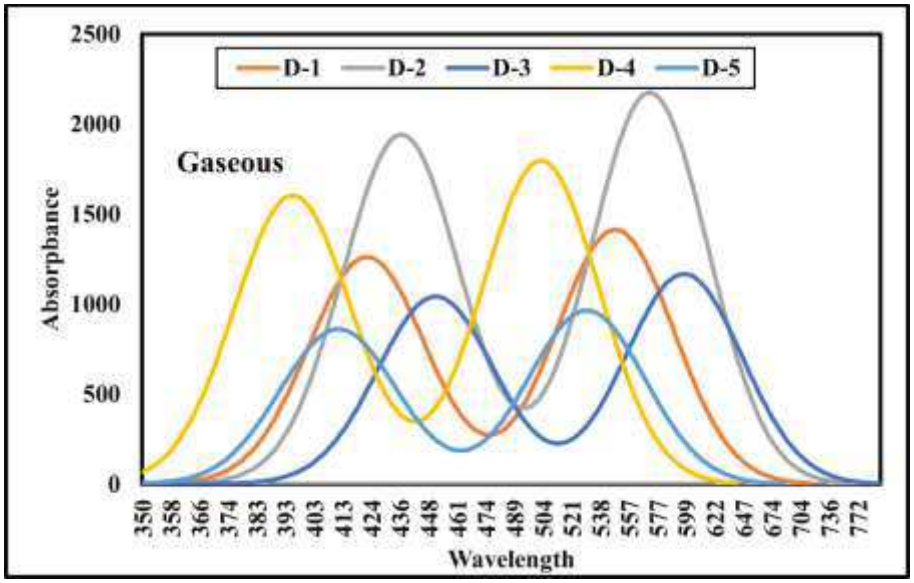

Fig. 6. Computed Uv-vis analysis of reference new dyes **(D-1 to D-5)** in gas

This experimental measurement agrees well with the computationally estimated λ_{max} (401.63 nm) at the CAM-B3LYP/6-31G(d,p) level of theory using the CPCM model and chloroform as the solvent (Fig 7).

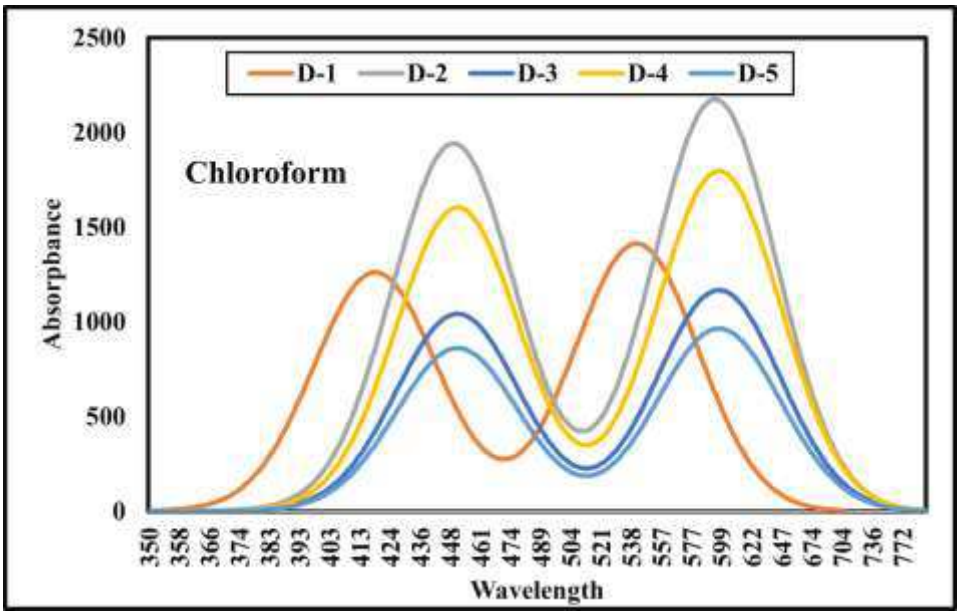

Fig. 7. Computed Uv-vis analysis of reference new dyes **(D-1 to D-5)** in chloroform

Because chloroform is commonly employed as a solvent in DSSCs, it has been used in next computations. The overall order of the λ_{max} values in chloroform was noted as: **D-3** (576) > **D-4** (545) > **D-2** (542) > **D-5** (532) > **D-1** (511) > **Ref-D** (465). The major electronic transitions that were noted for these λ_{max} values were HOMO-1→LUMO, HOMO→LUMO, HOMO→LUMO+1 and HOMO→LUMO+2. The computed λ_{max} in ethanol solvent is (405.1 nm), which is quite like the experimental data. The efficiency of cyanoacrylic acid and Si-containing anchoring groups has been compared using MO. At the same level of theory, the Ref-D was computed. The λ_{max} obtained experimentally is 398 nm in ethanol. The research of materials that collect photons of natural sunlight is known as light harvesting [39]. This encompasses research into the light-harvesting characteristics of photosynthetic systems developed and constructed to stimulate photochemical processes or create solar fuels. The collection of sunlight photons is a critical stage in the photosynthetic activity. The pigment-binding proteins operate as absorbed energies to promote photochemistry. The LHE of a newly designed materials can be calculated by the oscillator strength (*f*) of the λ_{max} values. In present study the Ref-D and all the new dyes had

the LHEs in descending order as: **D-2** (0.6154) > **D-3** (0.1169) > **D-4** (0.0984) > **Ref-D** (0.0922) > **D-1** (0.0518) >**D-5** (0.0078) (Table 4).

Table 4. Computed excited-state parameters of dye Ref-D and its new dyes **(D-1 to D-5)**

Dyes	State	E (eV)	λ	*f*	Major Transitions
Ref-D	1st	2.12	456	0.0512	HOMO-1→LUMO
	2nd	1.39	465	0.0420	HOMO→LUMO
	3rd	2.34	398	0.0230	HOMO→LUMO+1
D-1	1st	3.21	487	0.0123	HOMO→LUMO
	2nd	2.54	511	0.0231	HOMO→LUMO
	3rd	3.34	498	0.0032	HOMO-1→LUMO
D-2	1st	2.45	502	0.0034	HOMO→LUMO
	2nd	1.56	542	0.415	HOMO→LUMO+1
	3rd	2.32	454	0.0303	HOMO→LUMO
D-3	1st	2.12	497	0.0510	HOMO-1→LUMO
	2nd	2.32	576	0.0540	HOMO→LUMO+2
	3rd	2.21	456	0.0320	HOMO→LUMO+1
D-4	1st	1.32	521	0.0430	HOMO→LUMO
	2nd	1.98	545	0.045	HOMO→LUMO
	3rd	2.87	432	0.009	HOMO-1→LUMO
D-5	1st	3.421	458	0.005	HOMO→LUMO
	2nd	2.76	532	0.0034	HOMO→LUMO+1
	3rd	2.21	467	0.0043	HOMO-1→LUMO

The computed λ_{max} in gaseous state was (405.1 nm), which is quite like the experimental data. Furthermore, the efficiency of cyanoacrylic acid for anchoring groups was compared using an experimentally confirmed dye with *N*,*N*-dimethylaniline as the donor, thiophene as the π-spacer, and cyanoacrylic as the anchoring part. The dye **Ref-D** was computed at the same level. The λ_{max} found experimentally is 398 nm in ethanol solvent. This test result corresponds to the computed λ_{max} (401.63 nm) for the CAM-B3LYP/6-31G(d,p) level using CPCM and chloroform as solvent.

Non-linear optical Response

For these types of title dyes to be used in the field of nonlinear optoelectronic investigations, with structural insights [40]. The bridging features leading in hyperpolarizability rise require FT-IR and FT-Raman spectrometric study [41]. When studying hyperpolarizability, the investigated material structural makeup is treated as a distinct dye material structures. Most of the new dyes with their polarizability and hyperpolarizability tensors (a.u.) could well be computed using the preceding equation [42]. To carry out the desired results, an unconstrained open-shell CAM-B3LYP/6-31G(d,p) was employed. The chemical configurations were completely altered without any framework limits thanks to the Gaussian 09W software analysis. More polarity was expected to result in a smaller energy difference between the HOMO and LUMO bandgaps, which were inversely linked to their dipole moment. A significant NLO reaction was implied by a reduced bandgap, improved linear polarizability, and higher hyperpolarizability [43]. Employing chloroform as an organic solvent as well as the IEF-PCM modelling in computational analysis employing the TD-DFT approaches. The newly designed dyes with semiconductor anchoring groups as electron acceptors were simulated for their UV/visible spectra. Polarizability is negatively correlated with the HOMO-LUMO energy gap. A small energy gap is referred to as polarization. Smaller bandgap, larger linear polarizability, and a substantial NLO reaction are all predicted by optical metrics including dipole moment, HOMO-LUMO electron transfer allocations, oscillation strength, and related quantum chemical properties. The relationship between λ_{max} and energy bandgap was inverted. As the strength of the electron-drawing acceptor moieties linked to the donor rises, the energy bandgap gets smaller. Due to the impact of charge carrier dye materials at the terminals of dyes framework, absorbance intensity shifts to the top side. The early excited states of freshly formed small-donor dye material dye materials had average polarizability values in the descending order as: **Ref-D** (543) > **D-1** (1092) > **D-2** (987) > **D-3** (1321) > **D-4** (1231) > **D-5** (997). The hyperpolarizability values were noted as in their descending order: **D-1** (134532) > **D-2** (124152) > **D-3** (98123) > **D-5** (34521) > **D-4** (23413) > **Ref-D** (10031).

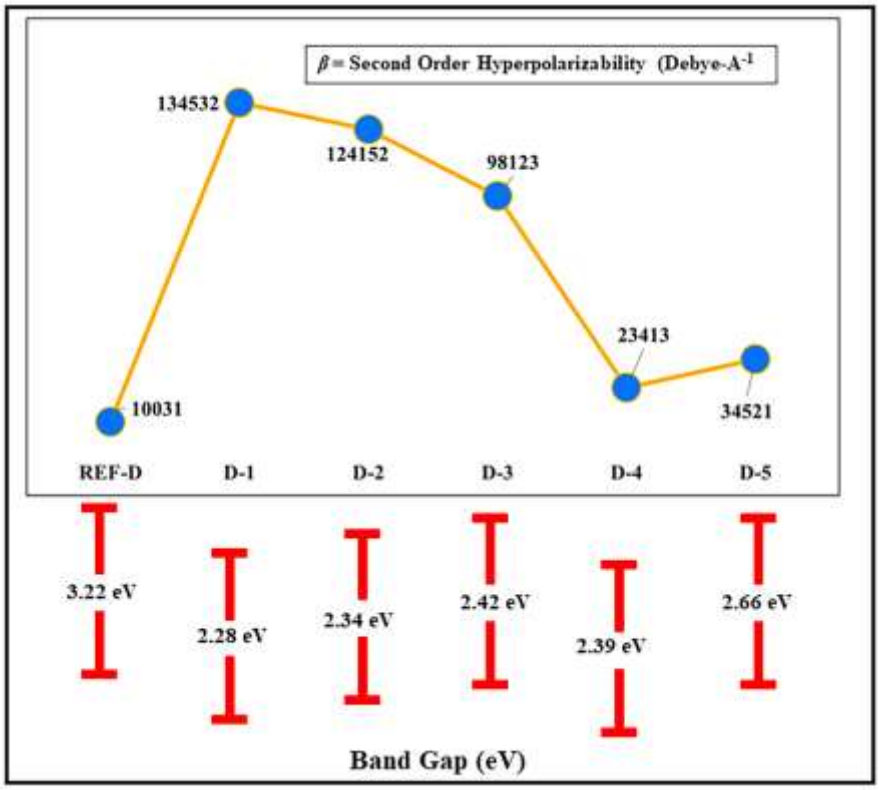

Fig.8. NLO analysis as a function of bandgap changes of reference new dyes **(D-1 to D-5)** in

The highest wavelength of the **MO** (reference) was 528 nm. To further understand the excited state charge transfer process, the wavelength maxima (λ_{max}) and energy transitions characteristics from the most occupied to the least occupied d-orbitals were measured for the six singlet excitons. There is a reciprocal link including λ_{max} and so excitation energy as the λ_{max} lowers and the excited states grows as we move from $S_1 \rightarrow S_n$ vibrational modes to $S_0 \rightarrow S_n$ excited singlet state. Regarding the excited states of S1Sn (n = 6), the Ref-D absorbance intensity was 519, 518, and 481 nm correspondingly. The bathochromic shift of the MO molecules is 488 nm, while the energy gap between the first and sixth singlet excited states is 0.869 eV. Due to its significant bandgap energy (E_g) and weak acceptor moiety, the Ref-D also displayed a small bathochromic shift in optical absorption. Low energy CT has showed significant CT values in NLO compounds with substantial transition moments and oscillator strengths.

$$\beta_{CT} = \frac{\Delta\mu_{gm} + f_{gm}}{E_{gm}^3} \qquad \text{(Eq. 7)}$$

The Ref-D reflectance peak was separated by 12.12 nm with λ_{max} at 669 nm due to 2.63 eV exciting energy fluctuations from $S_1 \rightarrow S_6$. The dyes D-3 and D-4 have absorption wavelengths by 217 nm and 191.03 nm, respectively, and have different excitation energies by 1.082 eV and 1.612 eV. The excitation energy from the excited state of $S_0 \rightarrow S_n$ (n = 6). The dye **D-4** had the easiest charge transfer since it has a greater excitation energy (1.32 eV) than the intended dyes that have the following descending order values: **D-5** (3.421) > **D-1** (3.21) > **D-2** (2.45) > **Ref-D** (2.12) > **D-3** (2.12) >**D-4** (1.32). The E is typically related to the energy needed for the first excitation. Because of the research, excitation energy is significantly lower than the bandgap energy of suggested dyes. A linear link exists between the energy bandgap and the excitation strengths. Widening the bandgap across HOMO and LUMO has several effects. The dipole moment is often associated with the stability of tiny organic solar cells in polar organic solvents. A higher dipole moment value improves the ability of OSC to process solutions. As a result, the solubility of a given dye material dye materials increases with increasing dipole moment, increasing material efficacy. The speedy and straightforward charge transfer is made easier by the highest maximum bending value, which also eases -conjugation. The dipole moment development of newly created dyess in their descending order was noted as: **Ref-D** (6.2036) > **D-2** (5.9726) > **D-1** (4.012) > **D-5** (3.7903) > **D-4** (3.4925) > **D-3** (2.6981). The production of donor components in identity thin film bulk heterostructure organic solar cell systems is significantly influenced by the dipole moment. While f_m^g stands in for the excited state dipole moment, f_m^g stands for the ground state dipole moment. Second-order polarizability is intrinsically linked towards the polarizability. Oscillator strength in the ground state as well as absorption across nth wavelength range (nm). Relationship between total (blue line) and matching CT (red line) values for D-5. The process that may occur in the cube, E_m^{3g}, is inversely proportional to β while the excited state f_m^g, is proportional to ß. Large oscillator intensity and transitional moments have been seen in NLO compounds with low energy CT.

Molecular Packing and Charge Tripping

The phase dispersion is controlled by the donor-acceptor miscibility, which affects the NLO and other photovoltaic properties in luau of their ability to trip the charges [44]. To get information about amorphous miscibility, the extent of molecular interaction of charge transport materials must be quantified. Miscibility assessment is quite useful in achieving the film shape (Fig. 9).

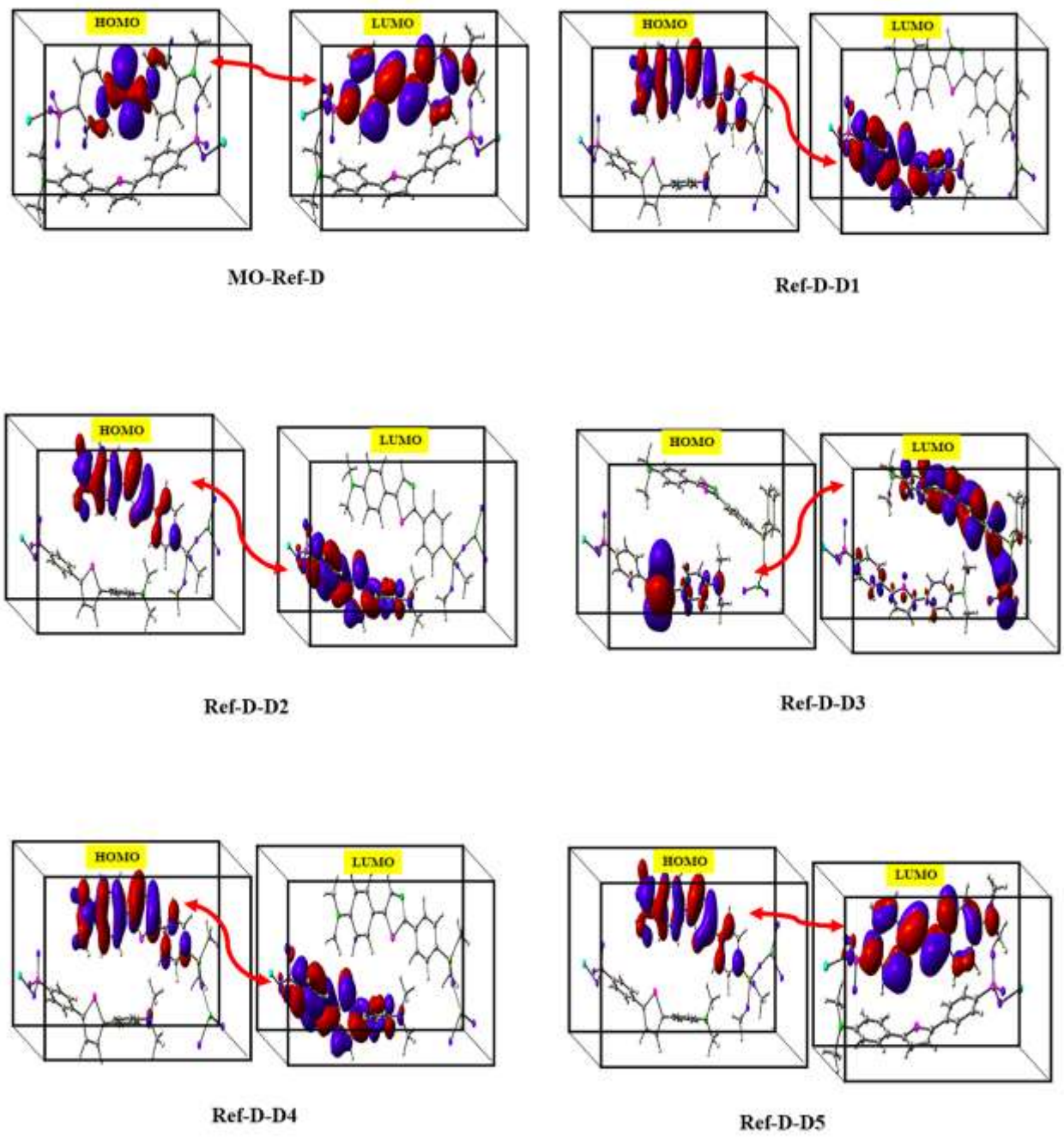

Fig. 9. Charge tripping analysis of new dyes **(D-1 to D-5)** by optimizing their complexes at DFT level

It has been stated that the best device photovoltaic properties may be achieved with the best miscibility and hence the best. All the newly developed dyes have been simulated for their miscibility and molecular studies by optimizing them at APFD level of DFT. The miscibility related quantum chemical parameter tends difficult to decide experimentally as there are several

approaches and a broad range of values for OSC devices are documented. Computational approaches are alternative ways for calculating the compressibility of a selected set of dye materials. The Blend module supplies many pair combinations for blending dye s. From their simulation boxes the tripping of charges from the HOMO of Ref-D to the LUMOs of the respective dyes can be seen.

Density of states

Implementing the FMO concepts for their outcomes benefits from an examination of the Density of States of freshly generated dye. Estimated DOS spectra at CAM-B3LYP/6-311G(d,p) [45] . The evidence bought by FMOs was supported the DOS studies. The DOS profiles of the compounds under investigation are shown in Figure 6, which makes it obvious if a moiety's significant acceptor character alters the pattern of dispersion around the HOMO and LUMO. To illustrate the DOS study, we divided our dyes into two parts: the donor (the core unit) and acceptor (the end-capped group), which have been depicted by red and green lines, respectively. On the x-axis, the electronic framework at LUMOs was represented by positive numbers, while the dielectric loss at HOMO was depicted by negative values. The distance here between two was used to depict the energy gap. It is helpful to look at the Density of States of newly created dye before implementing the FMO ideas for their effects. Figure 6 depiction of the dyes under investigation's DOS profiles makes it clear if a moiety's strong acceptor character affects the arrangement of dispersion surrounding the HOMO and LUMO. Our dyes were split into two groups for the DOS study: the donor (the core unit) and acceptor (the end-capped group), which are shown by red and green lines, correspondingly. Positive quantities on the x-axis denoted the electrical structure at LUMOs, while negative numbers showed the dielectric loss at HOMO.

Electron hole injection

We are investigating a hole/electron injection barrier (HIE/EIE) from dyes towards the Al electrode as (HIE = W of metal (E_{HOMO}) and (EIE = E_{LUMO} (W of metal). The declining order shown by the HIE of Ref-D and its new dyes for Au metal, the potential in descending order was seen as: **Ref-D** (0.89) > **D-2** (-1.67) > **D-5** (-1.72) > **D-3** (-1.75) > **D-1** (-1.76) > **D-4** (-1.77). The same trend noted for Al electrode was seen as: **D-5** (4.44) > **D-3** (4.23) = **D-4** (4.23) > **D-1** (4.1) > **D-2** (4.06) > **Ref-D** (2.5).

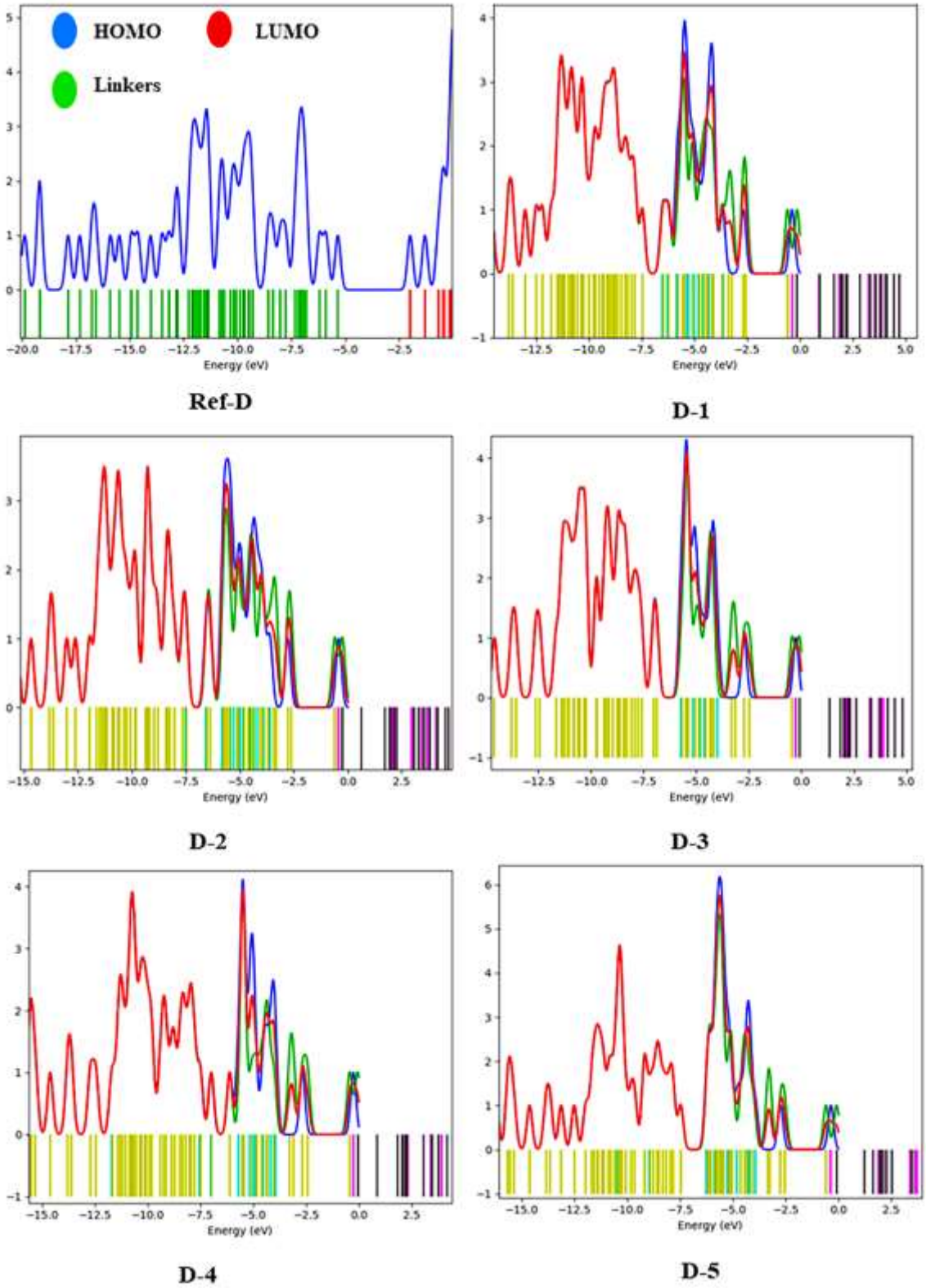

Fig. 10. Density of States analysis of dye Ref-D and its new dyes **(D-1 to D-5)**

The trend for (Au) and (Al) for EIE of **MO** and its newly developed dyes also offered some intriguing results, with (Au) reported with the same pattern as: **Ref-D** (9.51) > **D-2** (6.95) > **D-5** (6.9) > **D-3** (6.87) > **D-1** (6.86) > **D-4** (6.85). The Al electrode contrasted the subsequent tendency with one that was completely different, presenting it as: **D-5** (4.16) > **D-3** (3.95) > **D-4** (3.95) > **D-1** (3.82) > **D-2** (3.78) > **Ref-D** (2.22) .The majority of dyes may function as excellent electrode materials, and the influence of the electrode is essentially nonexistent, according to the electron injection and hole analyses. They likewise reflect a metal tendency that is identical. Therefore, it may be inferred that while Al would be an excellent electrode material for investigations involving electron injection, Au can become a good possibility for electron holes (Table 5).

Table 5. electron Injection and Hole analysis dye Ref-D and its new dyes **(D-1 to D-5)**

Dyes	**HIE (Au)**	**EIE(Au)**	**HIE (Al)**	**EIE (Al)**
Ref-D	0.89	2.50	9.51	2.22
D-1	-1.76	4.10	6.86	3.82
D-2	-1.67	4.06	6.95	3.78
D-3	-1.75	4.23	6.87	3.95
D-4	-1.77	4.23	6.85	3.95
D-5	-1.72	4.44	6.90	4.16

NBO analysis

Calculations of the distribution of electron densities across elements as well as the bonds that connect them are done using naturally localized orbitals. A method for finding acceptors and donors in various regions of the material is called NBO monitoring. This strategy can only be used to bring dye electrons through into semiconductor bandgap when the C group acts as an anchoring factor. The dyes D-1 and D-2 in the dyes, as well as the **MO** itself, had negative NBO driven energies. The dyes D-1 and D-2 have fewer negative values than the **MO**, which suggested that a negative charge is transferred from **MO** to the newly established dyes D -1 to D-5 during loading, according to Table 5. The study revealed that electronic densities were efficiently conveyed between donor through acceptor, resulting in an efficient charge condition where the most of donor and π-conjugated intermediate products had positive properties while all acceptors showed

negative values. The enhanced charge transfer capabilities are found in the dyes with the greatest NBO values of energetic for the π-conjugated bond length, while variants with the lowest value have been researched. Each dye that was produced appeared to work well with others.

Table 6. NBO analysis of dye Ref-D and its new dyes **(D-1 to D-5)**

Dye	donor (i)	Type	acceptor (j)	Type	$E^{(2)}$	E(j)E(i) (au)	$F_{i,j}$ (au)
D-1	Ti1-O2	π	Ti1-S12	π*	0.28	0.38	0.013
	Ti1-O2	π	Ti1-O3	π*	1.35	0.60	0.036
	Ti1-O2	π	Ti1-O22	π*	1.21	0.59	0.034
	Ti1-O3	π	Ti1-O2	π*	1.31	0.60	0.035
	S24	LP	C23-C25	π*	8.78	0.26	0.060
D-2	Ti1-O3	π	Ti1-O22	π*	1.17	0.59	0.033
	Ti1-O22	π	Ti1-S11	π*	0.56	0.40	0.019
	Ti1-O22	π	Ti1-O2	π*	1.36	0.62	0.037
	N4-C5	π	N4-C6	π*	1.91	0.93	0.053
	N4-C5	π	N4-C7	π*	1.56	0.95	0.049
D-3	N4-C5	π	C6-N36	π*	0.64	0.99	0.032
	S24	LP	C26-N27	π*	10.63	0.23	0.063
	N4-C5	π	C7-C8	π*	1.14	0.65	0.037
	N4-C6	π	N4-C5	π*	1.90	0.93	0.053
D-4	N4-C6	π	N4-C7	π*	1.64	0.95	0.050
	N27	LP	C23-C25	π*	1.52	0.91	0.034
	Ti1	π	Ti-O3	π*	0.47	1.97	0.038
	Ti1	π	Ti-O2	π*	0.25	1.99	0.028
	O22	π	Si19-O20	π*	6.51	0.38	0.064
	O22	π	Si19-O21	π*	3.71	0.37	0.048
D-5	N4-C6	π	C5-H32	π*	0.64	0.99	0.032
	N27	LP	C13-C26	π*	1.10	0.76	0.037
	N27	LP	C23-C25	π*	1.52	0.91	0.048

Electrostatic potentials

The locations of proposed combination' electron donating substitutions are revealed by molecular electrostatic potential (MEP) analyses, which enable the prediction of reactive species. B3LYP/SDD/6-31G(d,p) was used to decide the MEPs of the investigated **MO** and thus its newly produced dyes in Figure 13. The colors red, blue, and green, respectively, reflect the negative, positive, and neutral sections of the MEP regions. Nitrogen atoms are the focus of the negative region (red), which suggests that such regions are vulnerable to electrophilic assaults. The carbon and hydrogen atoms of CP/CP*, as well as those of dyes, are all covered by the positive (blue) zone, showing that nucleophilic interactions are possible at these sites. The parts of the dye material with no electrostatic charge are said to be neutral.

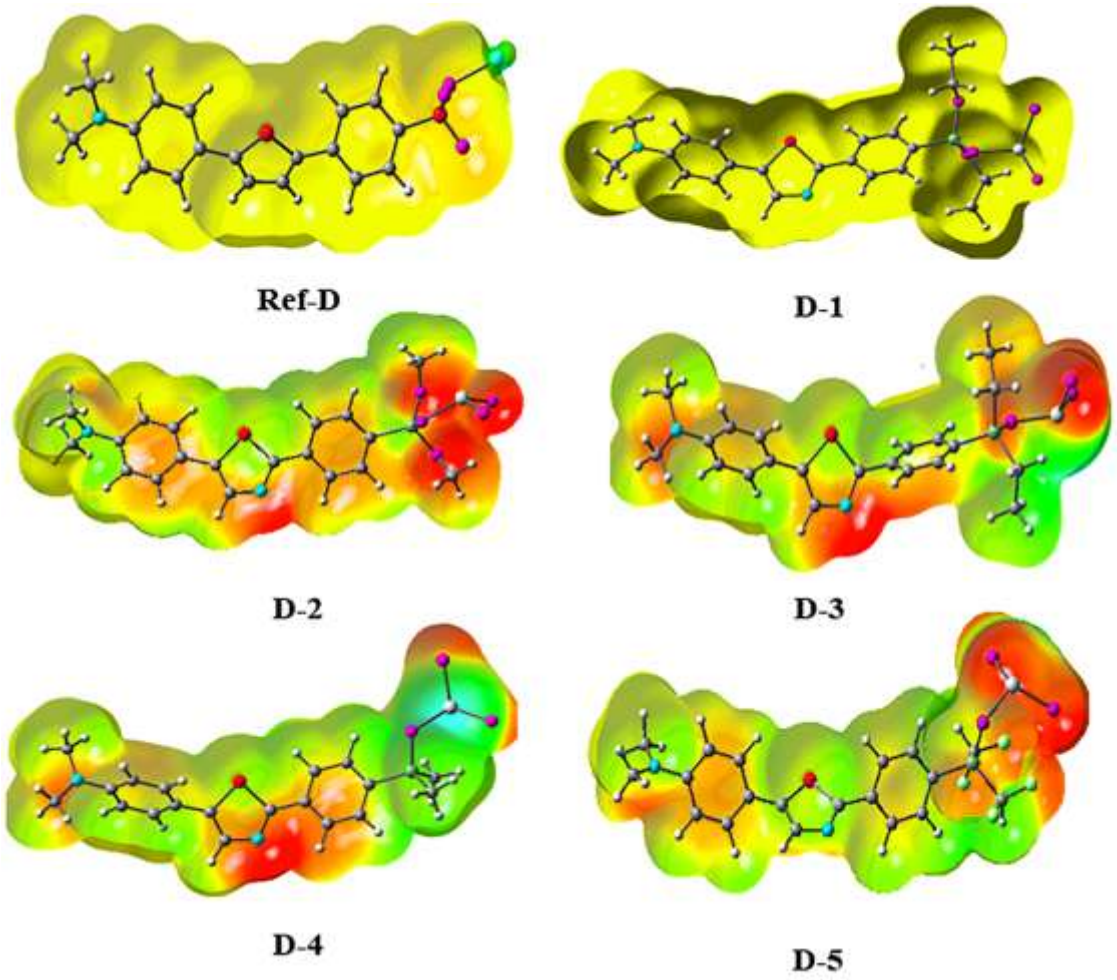

Fig. 11. Fig. 11Electrostatically mapped surfaces of Ref-D and its new dyes (**D-1 to D-5**)

Conclusions

While in opto-electronic industry, organic materials with notable nonlinear optical (NLO) characteristics are often used. By adjusting the various electronic group replaced chances to regulate their bandgap structure and their NLO sensitivities, nine newly created Pull-Push dyes with a D-$\boldsymbol{\pi}$-D- $A_{(Semiconductor)}$ framework were theoretically constructed from acceptor and donor components with π-spacers. Investigated is how different acceptors affect nonlinear kinetic energy modes. According to FMO testing, all the developed dyes showed extremely narrow bandgaps (0.65-2.42 eV), which had an impact on their other photovoltaic characteristics. Global reactivity traits were shown to be related to lower values, higher ratings, and a narrower bandgap. The dyes displayed higher peak value and lower energy electronics interactions in the UV-vis band when comparing to the benchmark dye material. The production of electrostatic interaction in dyes in between donor (D) and acceptor (A) species was shown by an NBO research. Charge transport from D to A may have caused a large NLO reaction that led to this charge separation. The dyes had initial hyperpolarizability indices that were eight times greater than the standard. Our research should contribute to the creation of organic dyes with favorable properties for enhancing optical device performance. Additionally, by applying pi-poor vs pi-rich semiconductor dyes to the dye-sensitive solar panels, a pull-push effect may be created to improve the NLO response.

Supplementary Information

The online version has supplementary material available at

Acknowledgements

The authors are grateful to the University of Gujrat, Gujrat, Pakistan for accessing the all-research facilities.

Contributions

Dr AUH: Conception and design of the study, acquisition of data and drafting the manuscript.
Dr SHS: Resources, supervision, edited the manuscript and provided valuable discussions and formal analysis
Dr MZ: Formal analysis
Dr GM: Softwires

Dr MFN: Validation

Dr MNZ: Editing the Maniscript

Data Availability

All data generated or analyzed during this study are included in this published article and its supplementary information file.

Code Availability

Gaussian 09 W and Gauss view 5.1 are used for simulation and origin software is used to draw the plots.

Ethics Declarations

This work did not involve any human subjects.

Consent to participate

This article does not have any studies with human participants or animals, clinical trial registration or plant reproducibility performed by any author.

Ethics Approval

Not applicable.

Consent for publication

All authors have approved the paper and agree with its publication.

Funding

The authors declare that no funds, grants, or other support were received during the preparation of this manuscript.

Competing Interests

The authors have no competing interests to declare that are relevant to the content of this article.

References

1. Albrecht G, Ubl M, Kaiser S, et al (2018) Comprehensive study of plasmonic materials in the visible and near-infrared: linear, refractory, and nonlinear optical properties. Acs Photonics 5:1058–1067

2. Sudarsan V (2012) Optical materials: Fundamentals and applications. Funct Mater 285–322. https://doi.org/10.1016/B978-0-12-385142-0.00008-8

3. Irfan A, Al-sehemi AG, Assiri MA, Ullah S (2020) Materials Science in Semiconductor Processing Exploration the effect of metal and electron withdrawing groups on charge transport and optoelectronic nature of schiff base Ni (II), Cu (II) and Zn (II) complexes at molecular and solid-state bulk scale. Mater Sci Semicond Process 107:104855. https://doi.org/10.1016/j.mssp.2019.104855

4. Hassan AU, Mohyuddin A, Güleryüz C, et al (2022) Novel pull–push organic switches with D–π–A structural designs: computational design of star shape organic materials. Struct Chem. https://doi.org/10.1007/s11224-022-01983-3

5. Fthenakis V (2009) Sustainability of photovoltaics: The case for thin-film solar cells. Renew Sustain Energy Rev 13:2746–2750

6. Taha A, Farag AAM, Adly OMI, et al (2017) Synthesis, spectroscopic, DFT and optoelectronic studies of 2-benzylidene-3-hydroxy -1-(5,6-diphenyl-1,2,4-triazine-3-yl)hydrazine metal complexes. J Mol Struct 1139:31–42. https://doi.org/https://doi.org/10.1016/j.molstruc.2017.03.020

7. Wang P, Zakeeruddin SM, Comte P, et al (2003) Gelation of ionic liquid-based electrolytes with silica nanoparticles for quasi-solid-state dye-sensitized solar cells. J Am Chem Soc 125:1166–1167

8. Sun J, Liu Z, Yan C, et al (2019) Efficient construction of near-infrared absorption donor--acceptor copolymers with and without Pt (II)-incorporation toward broadband nonlinear optical materials. ACS Appl Mater \& interfaces 12:2944–2951

9. Lova P, Manfredi G, Comoretto D (2018) Advances in functional solution processed planar

1D photonic crystals. Adv Opt Mater 6:1800730

10. Dayan S, Kalaycioglu NO, Daran J, Poli R (2013) Synthesis and Characterization of Half-Sandwich Ruthenium Complexes Containing Aromatic Sulfonamides Bearing Pyridinyl Rings : Catalysts for Transfer Hydrogenation of Acetophenone Derivatives. https://doi.org/10.1002/ejic.201300266

11. Chen C-Y, Wang M, Li J-Y, et al (2009) Highly efficient light-harvesting ruthenium sensitizer for thin-film dye-sensitized solar cells. ACS Nano 3:3103–3109

12. Teh CM, Mohamed AR (2011) Roles of titanium dioxide and ion-doped titanium dioxide on photocatalytic degradation of organic pollutants (phenolic compounds and dyes) in aqueous solutions: A review. J Alloys Compd 509:1648–1660

13. Duerto I, Sarasa S, Barrios D, et al (2022) Enhancing the temporal stability of DSSCs with novel vinylpyrimidine anchoring and accepting group. Dye Pigment 203:110310. https://doi.org/https://doi.org/10.1016/j.dyepig.2022.110310

14. Horiuchi T, Miura H, Sumioka K, Uchida S (2004) High efficiency of dye-sensitized solar cells based on metal-free indoline dyes. J Am Chem Soc 126:12218–12219

15. Galoppini E (2004) Linkers for anchoring sensitizers to semiconductor nanoparticles. Coord Chem Rev 248:1283–1297

16. Gennari M, Légalité F, Zhang L, et al (2014) Long-lived charge separated state in NiO-based p-type dye-sensitized solar cells with simple cyclometalated iridium complexes. J Phys Chem Lett 5:2254–2258

17. Ak\in S, Aç\ikgöz S, Gülen M, et al (2016) Investigation of the photoinduced electron injection processes for natural dye-sensitized solar cells: the impact of anchoring groups. RSC Adv 6:85125–85134

18. Reynal A, Palomares E (2011) Ruthenium Polypyridyl Sensitisers in Dye Solar Cells Based on Mesoporous TiO2. Eur J Inorg Chem 2011:4509–4526. https://doi.org/https://doi.org/10.1002/ejic.201100516

19. Zhao J, Li Y, Lin H, et al (2015) High-efficiency non-fullerene organic solar cells enabled by a difluorobenzothiadiazole-based donor polymer combined with a properly matched small molecule acceptor. Energy \& Environ Sci 8:520–525

20. Durand RJ, Achelle S, Gauthier S, et al (2018) Incorporation of a ferrocene unit in the $π$-conjugated structure of donor-linker-acceptor (D-$π$-A) chromophores for nonlinear optics (NLO). Dye Pigment 155:68–74

21. Hara K, Sugihara H, Tachibana Y, et al (2001) Dye-sensitized nanocrystalline TiO2 solar cells based on ruthenium (II) phenanthroline complex photosensitizers. Langmuir 17:5992–5999

22. Huo L, Hou J (2011) Benzo [1, 2-b: 4, 5-b′] dithiophene-based conjugated polymers: band gap and energy level control and their application in polymer solar cells. Polym Chem 2:2453–2461

23. Ambrosio F, Martsinovich N, Troisi A (2012) What is the best anchoring group for a dye in a dye-sensitized solar cell? J Phys Chem Lett 3:1531–1535

24. Murakoshi K, Kano G, Wada Y, et al (1995) Importance of binding states between photosensitizing molecules and the TiO2 surface for efficiency in a dye-sensitized solar cell. J Electroanal Chem 396:27–34

25. Zhang L, Cole JM (2015) Anchoring groups for dye-sensitized solar cells. ACS Appl Mater \& interfaces 7:3427–3455

26. Masui H, Maitani MM, Fuse S, et al (2018) D--$π$--A Dyes that Contain New Hydantoin Anchoring Groups for Dye-Sensitized Solar Cells. Asian J Org Chem 7:458–464

27. Wang Y, Liao Q, Chen J, et al (2020) Teaching an old anchoring group new tricks: enabling low-cost, eco-friendly hole-transporting materials for efficient and stable perovskite solar cells. J Am Chem Soc 142:16632–16643

28. Song X, Yu H, Yan X, et al (2018) A luminescent benzothiadiazole-bridging bis (salicylaldiminato) zinc (II) complex with mechanochromic and organogelation properties. Dalt Trans 47:6146–6155

29. Kakiage K, Yamamura M, Fujimura E, et al (2010) High performance of Si--O--Ti bonds for anchoring sensitizing dyes on TiO2 electrodes in dye-sensitized solar cells evidenced by using alkoxysilylazobenzenes. Chem Lett 39:260–262

30. Kakiage K, Aoyama Y, Yamamura M, et al (2014) A novel alkoxysilyl azobenzene dye photosensitizer with alkylamino group for dye-sensitized solar cells. Silicon 6:123–127

31. Paramasivam M, Chitumalla RK, Jang J, Youk JH (2018) The impact of heteroatom substitution on cross-conjugation and its effect on the photovoltaic performance of DSSCs--a computational investigation of linear vs. cross-conjugated anchoring units. Phys Chem Chem Phys 20:22660–22673

32. Frisch MJ, Trucks GW, Schlegel HB, et al (2016) G16_C01. Gaussian 16, Revision C.01, Gaussian, Inc., Wallin

33. Hassan AU, Guleryuz C (2021) THEORETICAL EVALUATION OF THE PERMEABILITY OF DISCHARGE ITEM (LiOOH) IN Li-O-2 BATTERIES. Lat Am Appl Res 51:153–157

34. Hassan AU, Sumrra SH, Imran M, Chohan ZH (2022) New 3d Multifunctional Metal Chelates of Sulfonamide: Spectral, Vibrational, Molecular Modeling, DFT, Medicinal and In Silico Studies. J Mol Struct 132305. https://doi.org/https://doi.org/10.1016/j.molstruc.2021.132305

35. Sumrra SH, Hassan AU, Zafar MN, et al (2022) Metal incorporated sulfonamides as promising multidrug targets: Combined enzyme inhibitory, antimicrobial, antioxidant and theoretical exploration. J Mol Struct 1250:131710. https://doi.org/https://doi.org/10.1016/j.molstruc.2021.131710

36. Luo J, Xue ZQ, Liu WM, et al (2006) Koopmans' theorem for large molecular systems within density functional theory. J Phys Chem A 110:12005–12009

37. Hassan AU, Sumrra SH, Raza MA, et al Design, facile synthesis, spectroscopic characterization, and medicinal probing of metal-based new sulfonamide drugs: A theoretical and spectral study. Appl Organomet Chem n/a:e6054.

https://doi.org/10.1002/aoc.6054

38. Fantin PA, Barbieri PL, Neto AC, Jorge FE (2007) Augmented Gaussian basis sets of triple and quadruple zeta valence quality for the atoms H and from Li to Ar: Applications in HF, MP2, and DFT calculations of molecular dipole moment and dipole (hyper) polarizability. J Mol Struct THEOCHEM 810:103–111

39. Zhang F, Wu D, Xu Y, Feng X (2011) Thiophene-based conjugated oligomers for organic solar cells. J Mater Chem 21:17590–17600. https://doi.org/10.1039/C1JM12801A

40. Sumrra SH, Hassan AU, Imran M, et al (2020) Synthesis, characterization, and biological screening of metal complexes of novel sulfonamide derivatives: Experimental and theoretical analysis of sulfonamide crystal. Appl Organomet Chem 34:e5623. https://doi.org/10.1002/aoc.5623

41. Noreen S, Sumrra SH (2022) Correlating the charge transfer efficiency of metallic sulfa-isatins to design efficient NLO materials with better drug designs. BioMetals. https://doi.org/10.1007/s10534-022-00385-6

42. Hassan AU, Mohyuddin A, Nadeem S, et al (2022) Structural and Electronic (Absorption and Fluorescence) Properties of a Stable Triplet Diphenylcarbene: A DFT Study. J Fluoresc. https://doi.org/10.1007/s10895-022-02969-4

43. Noreen S, Sumrra SH (2021) Aminothiazole-Linked Metal Chelates: Synthesis, Density Functional Theory, and Antimicrobial Studies with Antioxidant Correlations. ACS omega 6:33085–33099

44. Park SY, Park GE, Choi S, et al (2017) Effect of acceptor strength in new acceptor--donor--acceptor-type molecules on their miscibility with donor polymers for bulk-heterojunction fullerene-free solar cells. Dye Pigment 146:226–233

45. Moroz A (1995) Density-of-states calculations and multiple-scattering theory for photons. Phys Rev B 51:2068

Supplementary Files

This is a list of supplementary files associated with this preprint. Click to download.

- SFile.docx